Intermediate state polarization in multiphoton ionization of HCl

A. I. Chichinin
*Institut für Physikalische und Theoretische Chemie, Technische Universität Braunschweig,
38106 Braunschweig, Germany and Institute of Chemical Kinetics and Combustion,
630090 Novosibirsk, Russia*

P. S. Shternin
Ioffe Institute, Russian Academy of Sciences, 194021 St. Petersburg, Russia

N. Gödecke, S. Kauczok, and C. Maul[a)]
*Institut für Physikalische und Theoretische Chemie, Technische Universität Braunschweig,
38106 Braunschweig, Germany*

O. S. Vasyutinskii
*Institut für Physikalische und Theoretische Chemie, Technische Universität Braunschweig,
38106 Braunschweig, Germany and Ioffe Institute, Russian Academy of Sciences,
194021 St. Petersburg, Russia*

K.-H. Gericke
*Institut für Physikalische und Theoretische Chemie, Technische Universität Braunschweig,
38106 Braunschweig, Germany*

The paper presents the detailed theoretical description of the intermediate state polarization and photofragment angular distribution in resonance enhanced multiphoton ionization (REMPI) of molecules and the experimental investigation of these effects in the $E\,^1\Sigma^+$ and $V\,^1\Sigma^+$ states of HCl populated by two-photon transitions. It is shown that the intermediate state polarization can be characterized by the universal parameter b which is in general a complex number containing information about the symmetry of the two-photon excitation and possible phase shifts. The photofragment angular distribution produced by one- or multiphoton excitation of the polarized intermediate state is presented as a product of the intermediate state axis spatial distribution and the angular distribution of the photofragments from an unpolarized intermediate state. Experiments have been carried out by two complementary methods: REMPI absorption spectroscopy of rotationally resolved $(E,v'=0 \leftarrow X,v''=0)$ and $(V,v'=12 \leftarrow X,v''=0)$ transitions and REMPI via the $Q(0)$ and $Q(1)$ rotational transitions followed by three-dimensional ion imaging detection. The values of the parameter b determined from experiment manifest the mostly perpendicular nature of the initial two-photon transition. The experimentally obtained H^+-ion fragment angular distributions produced via the $Q(1)$ rotational transition show good agreement with theoretical prediction. © *2006 American Institute of Physics.* [DOI: 10.1063/1.2218336]

I. INTRODUCTION

The intriguing resonance enhanced multiphoton ionization (REMPI) of hydrogen halides, and of HCl in particular, has for decades been in the focus of interest of many laboratories[1–19] as an effective method for studying the structure of high-lying excited states and for monitoring chemical reaction products.

The theory of two-photon absorption of polarized light was developed by Bray and Hochstrasser,[20] Bain and McCaffery,[21] and Kummel *et al.*[22,23] The adaptation of this approach for atoms and convenient modifications of the obtained expressions were given by Bracker *et al.*[24] and by Smolin *et al.*[25] The corresponding expressions can be used for description of a 2+1 REMPI signal under the assumption that all intermediate state magnetic M substates are equally populated, and therefore the last ionization transition may

not be accounted for.[22] This approach is now widely used in REMPI polarization spectroscopy of the molecular excited states[10,26] and for investigation of the vector correlations in chemical reaction products.[16,27]

However, in general, the intermediate state magnetic M substates are not equally populated after a two-photon transition. The nonequilibrium population of the magnetic substates is equivalent to the intermediate state polarization (orientation and alignment)[28] and can dramatically change the photofragment angular distribution after the following ionization/dissociation transitions because the ionization/dissociation efficiency of the intermediate state can also be M dependent. This effect was recently studied for two-photon excitation of HCl by Manzhos *et al.*[18] who investigated the H atom photofragment angular distributions from dissociation of two-photon rovibronically state selected HCl and HBr prepared via a Q-branch transition. The expressions for the photofragment angular distribution following multi-

photon dissociation via near-resonant intermediate states of all possible symmetries have recently been presented by Dixon.[29]

The aim of this paper is to establish a detailed theoretical description of the intermediate state polarization effect in REMPI of molecules as a function of the incident light polarization and to perform the experimental investigation of this effect in the $E\,^1\Sigma^+$ and $V\,^1\Sigma^+$ excited states of HCl.

The theoretical analysis was a purely quantum mechanical one using the state multipole representation for both molecular and photon density matrices. Particularly, it was shown that the intermediate state polarization produced by a two-photon transition with a certain light polarization can be characterized by a universal parameter b which is in general a complex number containing information about the symmetry of the two-photon excitation and possible phase shifts. For an off-resonant two-photon excitation the parameter b is almost totally real and can be determined from the relative intensities of different two-photon absorption rotational transitions. Experimentally, the parameter b was determined through analysis of rotationally resolved absorption spectra of the $(E,v'=0\leftarrow X,v''=0)$ and $(V,v'=12\leftarrow X,v''=0)$ rovibrational branches and manifested in both cases a major contribution of the perpendicular character of the corresponding two-photon transitions. The values of the parameter b were then used for the calculation of the E and V state alignments.

A new expression for the photofragment angular distribution produced by one- or multiphoton excitation of the polarized intermediate state which can greatly simplify the analysis has been derived. Particularly, it is shown that in the axial recoil approximation the residual photofragment angular distribution can be presented as a product of the intermediate state axis spatial distribution and the angular distribution of the photofragments produced via photolysis from an unpolarized intermediate state. This means that the influence of the intermediate state polarization is independent of the particular multiphoton excitation mechanism.

This result is then applied to the photodissociation of HCl at dissociation wavelengths of 236 and 239 nm. For this system, Manzhos *et al.* have reported an anisotropy parameter of 1.04 for H^+ ions produced in the photodissociation of HCl with $J=1$,[18] whereas in a previous publication we have reported a value of 1.6 for H^+ originating from the photodissociation of HCl with $J=0$.[19] We have suggested before that this seeming contradiction may be due to alignment in the HCl molecule, and we will present evidence that this is indeed the case. In experiment, the angular distributions of H^+-ion fragments produced in REMPI of HCl have been studied at 236 and 239 nm by three-dimensional ion imaging. The REMPI process starts with two-photon resonant absorption producing the electronically excited states $HCl^*(E\,^1\Sigma^+,v=0)$ and $HCl^*(V\,^1\Sigma^+,v=12)$ via the Q rotational branch. Absorption of several more photons results in production of the H^+ fragments via different pathways which have been detected using a three-dimensional ion imaging technique.[19] The influence of the intermediate state alignment on the photofragment angular distribution has been analyzed by comparison of the H^+ ion angular distributions for $Q(0)$ and $Q(1)$ rotational transitions, having in mind that the $Q(0)$ transition

cannot produce any alignment. The obtained experimental results are found to be in good agreement with our theoretical predictions.

The paper is organized as follows.

Section II contains the main theoretical results of the paper, including the expression for the angular momentum polarization of the molecular excited state after two-photon excitation with its particular case of HCl excitation on the Σ-Σ electronic transition and the expression for the photofragment angular distribution after one- and two-photon dissociation.

Section III briefly discusses two complementary experimental setups used.

Section IV presents the main experimental results of our study of REMPI in HCl at 236 and 239 nm and their analysis and discussion. This includes

(1)   the analysis of the rotationally resolved absorption spectra of the $(E,v'=0\leftarrow X,v''=0)$ and $(V,v'=12\leftarrow X,v''=0)$ two-photon transitions and determination of the parameter b value and the intermediate alignment for both intermediate states, and

(2)   the analysis of the angular distributions of H^+-ion fragments and comparison of the obtained fitting parameters with theoretical prediction.

Section V contains the summary of the obtained results.
The derivation of all obtained theoretical expressions are given in Appendixes A–C.

II. THEORY

A. Angular momentum polarization of the molecular excited state after two-photon excitation

We consider the general case of two-photon excitation of a molecule from its initial state $|i\rangle$ to the excited state $|f\rangle$ by polarized light. Assuming that the light intensity is small, the equation of motion for the molecular density matrix $\rho_{f'f}$ can be written as

$$\frac{d\rho_{f'f}}{dt} = F_{f'f} - \frac{1}{\tau}\rho_{f'f}, \tag{1}$$

where f is the set of quantum numbers of the molecular excited state, τ is the lifetime, and $F_{f'f}$ is the excitation matrix which is given by the second order perturbation theory expression

$$F_{f'f}$$

$$= F_0 \sum_{i,i',e,e'} \frac{\hat{V}_{fe}^*\hat{V}_{ei}^*\hat{V}_{f'e'}\hat{V}_{e'i'}}{(\omega_{ei}-\omega+i(\Gamma_e/2))(\omega_{e'i'}-\omega-i(\Gamma_{e'}/2))}\rho_{i'i}, \tag{2}$$

where F_0 is a constant proportional to the square of the light intensity, $\rho_{i'i}$ is the initial state density matrix, and $\hat{V}$ is the standard interaction operator $\hat{V}=\mathbf{d}\cdot\mathbf{e}$, where $\mathbf{d}$ is a molecular dipole moment and $\mathbf{e}$ is the light polarization vector.

Summation in Eq. (2) proceeds over all quantum numbers of the initial (i,i') and intermediate (e,e') states. In the

case of a diatomic molecule, the initial state wave function can be detailed as $|i\rangle \equiv |n_i, \Omega_i, v_i, J_i, M_i\rangle$, where J_i is a total angular momentum, M_i and Ω_i are projections of J_i onto the laboratory and internuclear axes, respectively, v_i is a vibrational quantum number, and n_i is a set of additional quantum numbers which depends on further details of the angular momentum coupling. Similar expressions stand for the wave functions of the intermediate $|e\rangle$ and the excited $|f\rangle$ states.

It is convenient to formulate Eqs. (1) and (2) in terms of the state multipoles which are the irreducible representation of the density matrix and defined as [30,31]

$$\rho_{KQ}(JJ')$$
$$= \sum_{M,M'} (-1)^{J-M} \sqrt{2K+1} \begin{pmatrix} J & J' & K \\ M & -M' & -Q \end{pmatrix} \rho_{J'M'JM}, \quad (3)$$

where the term in parentheses is a $3j$ symbol.[32]

In the case of a diatomic molecule, the density matrix $\rho_{J'M'JM}$ and the state multipole $\rho_{KQ}(JJ')$ in Eq. (3) depend also on the quantum numbers Ω, Ω' which are dropped for brevity.

The inverse transformation is given by

$$\rho_{J'M'JM}$$
$$= \sum_{KQ} (-1)^{J-M} \sqrt{2K+1} \begin{pmatrix} J & J' & K \\ M & -M' & -Q \end{pmatrix} \rho_{KQ}(JJ'). \quad (4)$$

By combining Eqs. (2)–(4) and applying the angular momentum algebra in a way analogous to Ref. 22–24, Eq. (1) can be rewritten in the form

$$\frac{d\rho_{K_f Q_f}(J_f J'_f)}{dt} = F_{K_f Q_f}(J_f J'_f) - \frac{1}{\tau} \rho_{K_f Q_f}(J_f J'_f), \quad (5)$$

where the irreducible component of the excitation matrix $F_{K_f Q_f}(J_f J'_f)$ in the case of linearly or circularly polarized light can be written as (see Appendixes A and B):

$$F_{K_f Q_f}(J_f J'_f) = F_0 \sum_{K K_i} [C_K(\mathbf{n}_{ph}) \otimes \rho_{K_i}(J_i J'_i)]_{K_f Q_f} R^{K_f}_{K K_i}, \quad (6)$$

where $C_{KQ}(\mathbf{n}_{ph}) = [4\pi/(2K+1)]^{1/2} Y_{KQ}(\mathbf{n}_{ph})$ is a modified spherical harmonic and the vector $\mathbf{n}_{ph}$ is parallel to the direction of the light polarization vector $\mathbf{e}_{ph}$ in the case of linearly polarized light and to the direction of light propagation in the case of circularly polarized light. The factor in the square brackets in Eq. (6) is the irreducible tensor product[32]

$$[C_K(\mathbf{n}_{ph}) \otimes \rho_{K_i}(J_i J'_i)]_{K_f Q_f}$$
$$= \sum_{Q, Q_i} C^{K_f Q_f}_{KQ K_i Q_i} C_{KQ}(\mathbf{n}_{ph}) \rho_{K_i Q_i}(J_i J'_i), \quad (7)$$

where $C^{K_f Q_f}_{KQ K_i Q_i}$ is a Clebsch-Gordan coefficient.

The modified spherical harmonic $C_{KQ}(\mathbf{n}_{ph})$ of rank K describes the polarized photons. Rank K is limited to the values $K = 0, 2, 4$ in the case of linearly polarized light and to the values $K = 0, 1, 2, 3, 4$ in the case of circularly polarized light. The state multipole $\rho_{K_i Q_i}(J_i J'_i)$ with rank K_i and projection Q_i describes the initial state orientation and alignment. Rank K_i can take all positive integer values from $|J_i - J'_i|$ to $J_i + J'_i$. The state multipoles with $J_i \neq J'_i$ describe possible (J_i, J'_i) coherence in the initial state.[31] The excited state rank K_f can take all positive integer values from $|J_f - J'_f|$ to $J_f + J'_f$.

The scalar factor $R^{K_f}_{K K_i}$ in Eq. (6) depends on the angular momenta involved in the two-photon transition, but not on their projections and can be presented as

$$R^{K_f}_{K K_i} = \sum_{RR', J_i J'_i} \sqrt{(2K_i+1)(2R'+1)(2R+1)(2J'_i+1)(2J_i+1)(2J'_f+1)(2J_f+1)} (-1)^{J'_f - J_f} (2K+1)$$
$$\times \begin{Bmatrix} J_i & J_f & R \\ J'_i & J'_f & R' \\ K_i & K_f & K \end{Bmatrix} \begin{pmatrix} R & R' & K \\ 2p & -2p & 0 \end{pmatrix} \begin{pmatrix} 1 & 1 & R \\ p & p & -2p \end{pmatrix} \begin{pmatrix} 1 & 1 & R' \\ -p & -p & 2p \end{pmatrix} \sum_{\gamma, \gamma'} \begin{pmatrix} J'_i & R' & J'_f \\ \Omega'_i & \gamma' & -\Omega'_f \end{pmatrix} \begin{pmatrix} J_i & R & J_f \\ \Omega_i & \gamma & -\Omega_f \end{pmatrix} S_{R'\gamma'} S^*_{R\gamma}, \quad (8)$$

where p is the cyclic projection of the transition dipole moment in the "photon frame" (see Appendix A), which is equal to $p = 0$ in the case of linear light polarization, and $p = 1$ and $p = -1$ in the case of right- and left-handed circular light polarization, respectively. Note that due to the form of the interaction operator as a scalar product $\mathbf{d} \cdot \mathbf{e} = (-1)^s d_p e_s \delta_{p,-s}$, the sign of the projection p is opposite to the sign of the projection of the light polarization vector s.

In case $p = 0$, each of the quantum number R, R' can take only the values R, $R' = 0, 2$ due to the symmetry of the $3j$ symbols, while in case $p = \pm 1$, they can only be equal to $R = R' = 2$. The scalar factor $R^{K_f}_{K K_i}$ does not contain the quantum numbers J_e and J'_e because summation over them has proceeded. This summation can cause only a minimal loss of accuracy because the denominator in Eq. (2) practically does not depend on the rotational structure splitting between the

energy levels J_e and J'_e.

The factors S_{R_γ} in Eq. (8) contain transition matrix elements and the energy denominator of second order time-dependent perturbation theory

$$S_{R\gamma}(\Omega_f, \Omega_i) = \sum_{q_1, q_2} (-1)^\gamma \sqrt{2R+1} \begin{pmatrix} 1 & 1 & R \\ q_2 & q_1 & -\gamma \end{pmatrix}$$
$$\times \sum_e \frac{\langle n_f \Omega_f | d_{q_2} | n_e \Omega_e \rangle \langle n_e \Omega_e | d_{q_1} | n_i \Omega_i \rangle}{\omega_{ei} - \omega - i\Gamma_e/2}$$
$$\times \langle v_f | v_e \rangle \langle v_e | v_i \rangle. \tag{9}$$

Equations (4)–(8) are general and describe the population of the excited state magnetic substates via two-photon absorption. They can be used for any direction of linear or circular light polarization. The practical convenience of Eqs. (5) and (6) is that they are diagonal over K_f and Q_f, and

therefore the solution in many cases can be easily obtained. An important feature of Eq. (6) is the complete separation between the scalar factors $R_{KK_i}^{K_f}$ and the tensor quantities in the photon-molecule vector product. In this form, the qualitative dependence of the signal on laser polarization can be studied without reference to the intensity factors $R_{KK_i}^{K_f}$:

If $K_f = Q_f = 0$, then $J_f = J'_f$, $\Omega_f = \Omega'_f$, $K = K_i$, and the excitation matrix $F_{K_f Q_f}(J_f J'_f)$ in Eq. (6) is proportional to the two-photon absorption intensity I which can be written in the form

$$I = \sqrt{2J_f + 1} F_{00}(J_f J_f) = F_0 \sum_K (C_K(\mathbf{n}_{\mathrm{ph}}) \cdot \rho_K(J_i J'_i)) P_K, \tag{10}$$

where the factor in the parentheses is a scalar product[32] of the tensors $C_{KQ}(\mathbf{n}_{\mathrm{ph}})$ and $\rho_{KQ}(J_i J'_i)$ and P_K is the line strength factor,[33]

$$P_K = (-1)^{J_f + J_i} \sum_{RR'} \sqrt{(2K+1)(2R'+1)(2R+1)(2J_i+1)(2J'_i+1)}(2J_f+1) \begin{Bmatrix} R & R' & K \\ J'_i & J_i & J_f \end{Bmatrix} \begin{pmatrix} R & R' & K \\ 2p & -2p & 0 \end{pmatrix} \begin{pmatrix} 1 & 1 & R \\ p & p & -2p \end{pmatrix}$$
$$\times \begin{pmatrix} 1 & 1 & R' \\ -p & -p & 2p \end{pmatrix} \sum_{\gamma, \gamma'} \begin{pmatrix} J'_i & R' & J_f \\ \Omega'_i & \gamma' & -\Omega_f \end{pmatrix} \begin{pmatrix} J_i & R & J_f \\ \Omega_i & \gamma & -\Omega_f \end{pmatrix} S_{R'\gamma'} S^*_{R\gamma}. \tag{11}$$

The expression for two-photon absorption intensity in Eq. (10) generalizes the result recently reported by Smolin *et al.*[25] to the case $J_i \neq J'_i$ (presence of the initial state $J_i J'_i$ coherence). In the case of linear or circular light polarization (not elliptical) and for $J_i = J'_i$, Eq. (10) is equivalent to more general expressions given by Kummel *et al.*,[22,23] Docker,[34] and Bracker *et al.*[24]

It is seen from Eq. (11) that if $J_i \neq J_f$, or $\Omega_i \neq \Omega_f$, both quantum numbers R and R' are limited to the value of 2 and no knowledge about the transition dipole matrix elements is needed for calculation of the ratio of the line strength factors P_K/P_0. However, for the Q rotational branch of HCl, the above conditions are not fulfilled; therefore R and R' can be equal either to 0, or to 2, and more detailed analysis is needed.

B. The symmetry of two-photon transitions in HCl

We consider two-photon absorption from the ground $X\,^1\Sigma_0^+$ state to the excited $B\,^1\Sigma_0^+$ state in a HCl molecule neglecting possible rotational alignment of the ground state. Therefore, the ground state multipole is equal to

$$\rho_{K_i Q_i}(J_i J'_i) = \delta_{K_i, 0} \delta_{Q_i, 0} \delta_{J_i, J'_i}(2J_i + 1)^{-1/2}, \tag{12}$$

and the expression for two-photon absorption in Eq. (10) can be written as

$$I = F_0 \rho_{00} P_0. \tag{13}$$

According to the properties of the $3j$ symbols in Eq. (11), only the $J_i = J_f$ (Q branch) and $J_i = J_f \pm 2$ (S and O branches) are allowed in absorption. If light is linearly polarized, the line strength factors P_0 for these rotational branches are

$$P_0^Q = \frac{\sqrt{2J_i+1}}{3} \left[|S_{00}|^2 + \frac{2}{5} \frac{J_i(J_i+1)}{(2J_i-1)(2J_i+3)} |S_{20}|^2 \right], \tag{14}$$

$$P_0^S = \frac{\sqrt{2J_i+1}}{5} \frac{(J_i+2)(J_i+1)}{(2J_i+1)(2J_i+3)} |S_{20}|^2, \tag{15}$$

$$P_0^O = \frac{\sqrt{2J_i+1}}{5} \frac{J_i(J_i-1)}{(2J_i-1)(2J_i+1)} |S_{20}|^2. \tag{16}$$

The Q-line strength factor in Eq. (14) contains both zeroth and second rank tensors S_{00} and S_{20}, respectively, having the former as a major contribution. The S- and O-line strength factors contain contribution only from the second rank tensor S_{20}. The intensity of the Q branch is larger than the intensity of other branches, in agreement with experiment.[15]

Using Eqs. (9) and (13)–(16), the branching ratio of the intensities of different rotational branches starting from the same initial state J_i can be written as

$$\frac{I_Q}{I_S} = \frac{10}{3} \frac{(2J_i+1)}{(J_i+2)} \left[|b|^2 \frac{(2J_i+3)}{(J_i+1)} + \frac{1}{5} \frac{J_i}{(2J_i-1)} \right], \tag{17}$$

$$\frac{I_Q}{I_O} = \frac{10}{3}\frac{(2J_i+1)}{(J_i-1)}\left[|b|^2\frac{(2J_i-1)}{J_i} + \frac{1}{5}\frac{(J_i+1)}{(2J_i+3)}\right]. \qquad (18)$$

These branching ratios depend on the square modulus of the parameter b,

$$b = \frac{S_{00}}{\sqrt{2}S_{20}} = \frac{D_\perp - D_\parallel}{D_\perp + 2D_\parallel}, \qquad (19)$$

where $D_\perp$ and $D_\parallel$ are two-photon transition moments:

$$D_\parallel = \sum_e \frac{\langle n_f,0|\hat{d}_0|n_e,0\rangle\langle n_e,0|\hat{d}_0|n_i,0\rangle}{\omega_{ei} - \omega - i(\Gamma_e/2)}\langle v_f|v_e\rangle\langle v_e|v_i\rangle, \qquad (20)$$

$$D_\perp = 2\sum_e \frac{\langle n_f,0|\hat{d}_1|n_e,-1\rangle\langle n_e,-1|\hat{d}_{-1}|n_i,0\rangle}{\omega_{ei} - \omega - i(\Gamma_e/2)}\langle v_f|v_e\rangle\langle v_e|v_i\rangle. \qquad (21)$$

The values $D_\perp$ and $D_\parallel$ represent contributions from the "parallel" $\Sigma\rightarrow\Sigma\rightarrow\Sigma$ and "perpendicular" $\Sigma\rightarrow\Pi\rightarrow\Sigma$ optical transitions, respectively.

In general, the parameter b is a complex number describing contributions from the parallel and perpendicular excitation pathways and possible phase shifts. Particularly, $b=1$ in the case of the pure perpendicular pathway, $D_\perp\neq 0$ and $D_\parallel=0$, and $b=-1/2$ in the case of the pure parallel pathway, $D_\perp=0$ and $D_\parallel\neq 0$. The expressions which are equivalent to Eqs. (14)–(18) have been reported by Bray and Hochstrasser[20] and Kummel et al.[22] who did not introduce the parameter b. Note that the values S_{00} and S_{20} in Eqs. (14)–(16) are denoted in Refs. 20 and 22 as μ_I and μ_S, respectively.

C. Excited state alignment: $\Sigma\leftarrow\Sigma$ transition

The alignment of the excited state $|f\rangle$ via a two-photon transition for any J_i and J_f values can be calculated using Eqs. (5) and (6) which in general contain possible initial state anisotropy. If the initial state is isotropic, the state multipole $\rho_{K_iQ_i}(J_iJ_i')$ is given in Eq. (12). Assuming that the light is linearly polarized along the Z axis, Eqs. (6) and (8) result in the steady state regime in the following expression for the excited state alignment:

$$\rho_{K_fQ_f}(J_fJ_f') = F_0\tau\delta_{K_f,K}\delta_{Q_f,0}\widetilde{P}_K, \qquad (22)$$

where the line strength factor $\widetilde{P}_K$ is

$$\widetilde{P}_K = (-1)^{J_i+J_f}\sum_{RR'}\sqrt{(2K+1)(2R'+1)(2R+1)(2J_f+1)(2J_f'+1)}\begin{Bmatrix}R' & R & K\\ J_f' & J_f & J_i\end{Bmatrix}\begin{pmatrix}R & R' & K\\ 0 & 0 & 0\end{pmatrix}\begin{pmatrix}1 & 1 & R\\ 0 & 0 & 0\end{pmatrix}$$
$$\times\begin{pmatrix}1 & 1 & R'\\ 0 & 0 & 0\end{pmatrix}\sum_{\gamma,\gamma'}\begin{pmatrix}J_i & R' & J_f'\\ \Omega_i & \gamma' & -\Omega_f'\end{pmatrix}\begin{pmatrix}J_i & R & J_f\\ \Omega_i & \gamma & -\Omega_f\end{pmatrix}S_{R'\gamma'}S_{R\gamma}^*. \qquad (23)$$

For $K_f=0$ and $Q_f=0$ the state multipole in Eq. (22) is proportional to the total number of the excited molecules, while the state multipoles with $K_f=1,2,\ldots$ describes orientation and alignment of the molecular angular momenta (see Ref. 31).

In the case of the $\Sigma\leftarrow\leftarrow\Sigma$ transition, both Ω_f and Ω_f' quantum numbers are equal to zero. If the excited state rotational states are well resolved in absorption, only the $J_f=J_f'$ terms should be preserved in Eq. (23). For a Q transition ($J_i=J_f$), the line strength factor $\widetilde{P}_K$ in Eq. (23) is equivalent to the line strength factor P_K in Eq. (11). Obviously, no alignment can be produced in the $Q(0)$ transition. For the $Q(1)$ transition, $J_i=J_f=1$ and Eqs. (22) and (23) can be rewritten as

$$\rho_{00} = \frac{C'}{3\sqrt{3}}\left(|S_{00}|^2 + \frac{4}{25}|S_{20}|^2\right) = \frac{2C'|S_{20}|^2}{3\sqrt{3}}\left(|b|^2 + \frac{2}{25}\right), \qquad (24)$$

$$\rho_{20} = -\frac{2C'}{75}\sqrt{\frac{2}{3}}\left(|S_{20}|^2 - \frac{10}{\sqrt{2}}\,\mathrm{Re}[S_{00}S_{20}^*]\right)$$
$$= -\frac{2C'|S_{20}|^2}{75}\sqrt{\frac{2}{3}}(1 - 10\,\mathrm{Re}[b]). \qquad (25)$$

As shown in Eqs. (24) and (25), only the ρ_{00} and ρ_{20} state multipoles differ from zero. The sign of the excited

state alignment, which is proportional to the ratio ρ_{20}/ρ_{00}, depends on the real part of the parameter b, $\mathrm{Re}[b]$. If $\mathrm{Re}[b] > 1/10$, the alignment of the molecular B state ρ_{20} is *positive*. This sign of alignment corresponds to the preferential population of the $M_J = \pm 1$ magnetic substates.

D. Photofragment angular distribution axes after multiphoton dissociation from the polarized state

The expression for the angular distribution of the photofragments produced by one-photon photolysis from a polarized molecular state has recently been reported by Underwood and Powis[35] as a particular case of their more general theory describing the photofragment angular momentum polarization. Underwood and Powis started with the expression for the photodissociation differential cross section and proceeded with some time-consuming angular momentum algebra manipulations.

However, in this paper, for considering the photofragment angular distribution, we use another and more simple approach which allows us to obtain the same result as that of Underwood and Powis[35] and readily generalize it to the case of multiphoton photodissociation. The main idea of this approach is treating the photodissociation step as a "normal" absorption transition, calculating the upper state density matrix and resulting molecular axis distribution. The unbound character of the upper (continuum energy) state can be taken into account by performing summation over all possible J, J' interference terms. Assuming axial recoil, the residual upper state molecular axis distribution is equivalent to the photofragment angular distribution.

The angular distribution of molecular axes $\omega(\mathbf{n})$ for a molecular quantum state described by the density matrix $\rho_{J'M'\Omega', JM\Omega}$ can be calculated from the expression

$$
\omega(\mathbf{n}) = \sum_{JJ'MM'\Omega} \rho_{J'M'\Omega' JM\Omega} \Psi_{J'M'\Omega'}(\phi, \theta, \gamma)
$$
$$
\times \Psi^*_{JM\Omega}(\phi, \theta, \gamma) \delta_{\Omega, \Omega'}, \tag{26}
$$

where $\Psi_{JM\Omega}(\phi, \theta, \gamma)$ is the rotational wave function of a diatomic molecule (Wigner D function[28]) and $\mathbf{n}$ is the direction of the molecular axis specified by the angles θ and ϕ. The indices Ω and Ω' are equal to each other because the angular distribution in Eq. (26) does not depend on the third Euler angle γ. For the Σ state the quantum number Ω is equal to zero.

If the J states are well resolved, only the $J = J'$ terms should be preserved in Eq. (26); however, in general, the coherent terms with $J \neq J'$ should also be accounted for. After transformation in Eq. (26) to the irreducible representation of the density matrix (3), it can be presented in the form

$$
\omega(\mathbf{n}) = \frac{1}{4\pi} \sum_{KJJ'\Omega} (-1)^{J'-\Omega} \sqrt{(2J+1)(2J'+1)}
$$
$$
\times C^{K0}_{J\Omega J'-\Omega} (\rho_K(J, J') \cdot C_K(\mathbf{n})). \tag{27}
$$

We obtained the angular distribution of photofragments produced by one or two-photon dissociation from the polarized intermediate state $|f\rangle$ into the group of "continuum en-

ergy" states $|c\rangle$ by calculating the continuum energy state multipoles $\rho_{K_c Q_c}(J_c J'_c)$ using Eq. (5) and substituting them into Eq. (27). The main assumption made is that the molecular axis does not rotate during the recoil time, which is equivalent to the known "axial recoil" approximation.[28] As mentioned above, for the continuum energy states all possible coherent terms with $J_c \neq J'_c$ were taken into consideration.

For one-photon excitation, the excitation matrix $F_{K_c Q_c}(J_c J'_c)$ is well known (see, e.g., Refs. 30 and 36), while for two-photon excitation it is given in Eq. (6) where the subscript indices f and i should be replaced by c and f, respectively.

Following this scheme, the photofragment angular distribution $\omega(\mathbf{n})$ produced by a multiphoton excitation via the intermediate state can be presented in the following simple form (see Appendix C):

$$
\omega(\mathbf{n}) = \omega_f(\mathbf{n}) \omega^{(k)}_{\mathrm{ph}}(\mathbf{n}, \mathbf{n}_{\mathrm{ph}}), \tag{28}
$$

where $\omega_f(\mathbf{n})$ is the angular distribution of the axes in the intermediate state $|f\rangle$ and $\omega^{(k)}_{\mathrm{ph}}(\mathbf{n}, \mathbf{n}_{\mathrm{ph}})$ is the photofragment angular distribution produced by k-photon photolysis of the unpolarized state $|f\rangle$.

Equation (28) is a pure quantum mechanical expression and is valid for any integer or half-integer value of the molecular angular momentum J_f. It manifests that the influence of the intermediate state alignment described by the first term is *independent* of the subsequent dissociation mechanism described by the second term.

In the case of HCl, the angular distribution of the molecular axes in the $B\,^1\Sigma$ state populated via the $Q(1)$ two-photon transition with linearly polarized light can be calculated from Eqs. (22), (24), and (27), holding $J_f = J'_f = 1$ and presented in the following traditional form:

$$
\omega_f(\mathbf{n}) = \frac{1}{4\pi}(1 + \beta^{(f)} P_2(\cos\theta)), \tag{29}
$$

where $P_2(\cos\theta)$ is the second order Legendre polynomial and the parameter $\beta^{(f)}$ is expressed by

$$
\beta^{(f)} = -\frac{\sqrt{2}\rho_{20}}{\rho_{00}} = \frac{2 - 20\,\mathrm{Re}[b]}{2 + 25|b|^2}. \tag{30}
$$

If $J_f > 1$, the axis angular distribution in Eq. (29) contains additional terms proportional to $P_k(\cos\theta)$, where $k = 4, 6, \ldots, J_f + J'_f$.

In the case of one-photon excitation the factor $\omega^{(1)}_{\mathrm{ph}} \times (\mathbf{n}, \mathbf{n}_{\mathrm{ph}})$ in Eq. (28) can be written as

$$
\omega^{(1)}_{\mathrm{ph}}(\mathbf{n}, \mathbf{n}_{\mathrm{ph}}) = \sum_{K_1 q} (-1)^{K_1 + q} (E_{K_1} \cdot C_{K_1}(\mathbf{n})) C^{K_1 0}_{1 q 1 - q}
$$
$$
\times \sum_{n_c \Omega_c} |\langle n_c \Omega_c | d_q | n_f \Omega_f \rangle \langle v_c | v_f \rangle|^2, \tag{31}
$$

where $E_{K_1 Q_1}$ is a photon polarization matrix with rank K_1 and projection Q_1 (Ref. 28) and the expression in the parentheses is a scalar product. The indices in the transition moment matrix element obey the selection rule $\Omega_f + q = \Omega_c$, where $\Omega_f = 0$ and the values $q = 0$ and $q = \pm 1$ correspond to the

parallel and perpendicular transitions from the $B\,^1\Sigma$ state to the continuum energy state, respectively.

Equation (31) is valid for an arbitrary direction of linear or circular light polarization. It is equivalent to the expression for zero-rank state multipole angular distribution given by Siebbeles *et al.*[37] If the light is linearly polarized along the Z axis, Eq. (31) results in the well-known expression $\omega_{\mathrm{ph}}^{(1)}(\mathbf{n}) \propto [1 + \beta_2^{(1)} P_2(\cos\theta)]$.[28]

In the case of two-photon excitation, the factor $\omega_{\mathrm{ph}}^{(2)}(\mathbf{n}, \mathbf{n}_{\mathrm{ph}})$ in Eq. (28) can be written as

$$\omega_{\mathrm{ph}}^{(2)}(\mathbf{n}, \mathbf{n}_{\mathrm{ph}}) = \sum_{Kp} \sum_{RR'} (C_K(\mathbf{n}_{\mathrm{ph}})$$

$$\times \cdot C_K(\mathbf{n})) C_{R2pR'-2p}^{K0} C_{1p1p}^{R2p} C_{1-p1-p}^{R'-2p}$$

$$\times \sum_\gamma (-1)^\gamma C_{R\gamma R'-\gamma}^{K0} S_{R'\gamma} S_{R\gamma}^*, \qquad (32)$$

which, for the light polarization along the Z axis, gives $\omega_{\mathrm{ph}}^{(2)}(\mathbf{n}) \propto [1 + \beta_2^{(2)} P_2(\cos\theta) + \beta_4^{(2)} P_4(\cos\theta)]$.
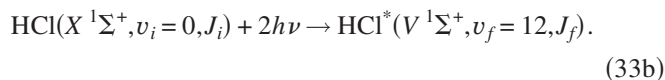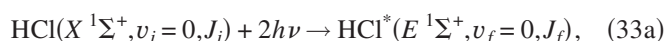
III. EXPERIMENT

The apparatus and technique have previously been described in detail[16,38] and here will be summarized only. Alignment effects in REMPI of HCl were studied with two complementary experimental setups. The first one was used to determine REMPI spectra of HCl$^+$; the second was used to obtain three-dimensional (3D) images of H$^+$ ions.

A. REMPI spectra of HCl$^+$

REMPI $(2+1_i)$ rotational spectra of HCl$^+$ were recorded in a one-dimensional time-of-flight (TOF) experiment, in which room-temperature HCl was admitted to a vacuum chamber under constant flow maintaining a pressure of 10^{-4} mbar. The dye laser (Lambda Physik FL 3000) was operated with Coumarin-47 at a repetition rate of 100 Hz; its light was frequency doubled by a beta-barium borate (BBO) crystal and focused by a 20 cm lens into the vacuum chamber. An excimer laser (Lambda Physik LPX 600) was used to pump the dye laser. Ions at masses 1, 35, 36, 37, and 38 resulting from various ionization and fragmentation schemes were detected independently by a double stage multichannel plate (MCP) assembly, and the corresponding transient TOF profiles were transferred to a digital oscilloscope (LeCroy 9450) and stored on a computer for further analysis. In such experiments rotationally resolved spectra were obtained and intensity ratios for O, Q, and S branch lines were determined. For the analysis of line intensities only spectra obtained for H^{35}Cl were used. All other masses showed identical spectral signatures, with well-known intriguing dependence of HCl fragmentation on excitation wavelength. Basically, for the shorter wavelengths fragmentation dominates over ionization, and for the longer wavelengths the situation is reversed. However, within the range covered by O, Q, and S transitions originating from the same rotational state, the fragmentation ratio was found to be unaffected by excitation wavelength.

Two vibrational transitions were studied,

$$\mathrm{HCl}(X\,^1\Sigma^+, v_i = 0, J_i) + 2h\nu \rightarrow \mathrm{HCl}^*(E\,^1\Sigma^+, v_f = 0, J_f), \quad (33a)$$

$$\mathrm{HCl}(X\,^1\Sigma^+, v_i = 0, J_i) + 2h\nu \rightarrow \mathrm{HCl}^*(V\,^1\Sigma^+, v_f = 12, J_f). \quad (33b)$$

We denote these transitions by $(E, 0\text{-}X, 0)$ and $(V, 12\text{-}X, 0)$. For the first one the wavelength was scanned from 238.5 to 239.4 nm covering the strong Q branch lines from $J_i = 0$ to 7 together with the much weaker O and S branches. For the second one the scanned wavelength range was 235.8–237.4 nm, where the Q branch was observed up to $J_i = 8$. The assignment of rotational lines of these transitions was taken from works of Green *et al.*[5–7,9] and Kvaran *et al.*[10]

B. 3D imaging of H$^+$

3D distributions of H$^+$ were observed by the Braunschweig 3D imaging machine. The experimental setup is identical to the one described in our previous publication.[19] It consists of a homebuilt single-field TOF mass spectrometer, a cold supersonic molecular beam, a position sensitive detector for ions, and an optic system based on a Nd:YAG (yttrium aluminum garnet) laser-pumped dye laser. In other words, we use a photofragment imaging technique in a single-laser configuration with a special position sensitive detector named delay-line detector. The transverse velocity components (v_x, v_y) of the initial velocity of each ion are determined from the measured two-dimensional impact position on the detector surface, while the measured time of arrival gives the longitudinal component (v_z) of the velocity. Hereafter the laboratory axes X, Y, and Z are directed along the laser beam, the molecular beam, and the accelerating electric field, respectively; they are mutually orthogonal. The electric vector of linear polarized laser radiation is denoted by $\mathbf{E}$; it is directed either along Z ($\mathbf{E} \| \mathbf{Z}$) or along Y ($\mathbf{E} \perp \mathbf{Z}$). The dye laser (Lambda Physik, Scanmate) was operated with Coumarin-47 at a repetition rate of 100 Hz; its light was frequency-doubled by a BBO crystal, separated by a Pellin-Broca prism and focused by a 20 cm lens into the ion chamber of the TOF mass spectrometer. The laser energy was kept low to obtain approximately one event per ten laser pulses to avoid kinetic energy transfer to the fragments due to space charge effects and to avoid saturation of the dissociation steps. The polarization of the laser was changed by a half-wave plate. Signals of the delay-line detector were digitized by time-to-digital converters, accumulated over 100–200 thousand laser shots and saved online by a personal computer.

H$^+$ ions were produced by the processes specified in the following section via the vibrational transitions $(E, 0\text{-}X, 0)$ and $(V, 12\text{-}X, 0)$ in which only $Q(0)$ $(J_i = J_f = 0)$ and $Q(1)$ $(J_i = J_f = 1)$ rotational transitions were used.

IV. EXPERIMENTAL RESULTS AND ANALYSIS

### A. Mechanism of HCl ionization and of H$^+$ production

The REMPI of HCl near 236 and 239 nm is studied by three-dimensional ion imaging. The first step of the REMPI process is the resonant two-photon absorption,

$$HCl(X\,^1\Sigma^+, v_i, J_i) + 2h\nu \rightarrow HCl^*(B\,^1\Sigma^+, v_f, J_f), \qquad (34)$$

which transfers the HCl molecule to the excited $B\,^1\Sigma^+$ state.

This excited state has two minima, since it is a mixture of the Rydberg $E\,^1\Sigma^+$ state with the valence $V\,^1\Sigma^+$ state. Thus, process (34) includes both transitions (33a) and (33b). Absorption of the next photons results in various processes resulting in H^+, Cl^+, and HCl^+ photofragments which have been the subject of study of many groups.[1–15,17,19,39–46]

In the previous paper[19] we determined the speed distributions and anisotropy parameters of H^+, Cl^+, and HCl^+ ions and used these data to analyze in detail the pathways for production of these ions. H^+ ions are produced via different pathways. The dominant pathway is the one-photon transition to repulsive superexcited states. These superexcited states may decay into two neutral fragments, either into a ground state $Cl(^2P)$ atom and an excited $H^*(n=2)$ atom,

$$HCl^* + h\nu \rightarrow HCl^{**}(^1\Sigma^+) \rightarrow Cl + H^*(n=2), \qquad (35)$$
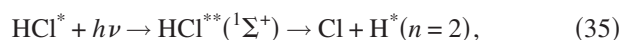
or into an excited state Cl^* atom and a ground state $H^*(n=1)$ atom,

$$HCl^* + h\nu \rightarrow HCl^{**}(^1\Sigma^+) \rightarrow Cl^* + H(n=1), \qquad (36)$$
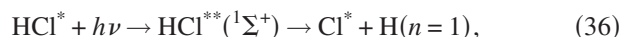
followed by the one-photon ionization of $H^*(n=2)$ or Cl^* atoms as a third step. There is experimental evidence for the occurrence of nonadiabatic transitions from these superexcited states to the ion pair state, resulting in the production of $H^+ + Cl^-$.[47]

$$H^*(n=2) + h\nu \rightarrow H^+ + e^-. \qquad (37)$$

Another channel producing H^+ ions is, instead of (35), the direct ionization of HCl^*,

$$HCl^*(B\,^1\Sigma^+) + h\nu \rightarrow HCl^+(X\,^2\Pi_\Omega) + e^-, \qquad (38)$$
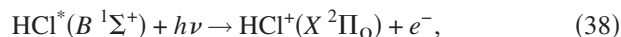
which produces the vibrationally excited ion HCl^+. Then, the third step is the photodissociation of HCl^+,

$$HCl^+(X\,^2\Pi_\Omega) + h\nu \rightarrow H^+ + Cl(^2P), \qquad (39)$$

which produces the H^+ ions. We say that HCl^+ ions are produced by REMPI $(2+1_i)$ in process (38) and that H^+ ions are produced by REMPI $(2+1+1_i)$ in processes (35) and (37) and by REMPI $(2+1_i+1)$ in processes (38) and (39), where the index i is added to label the ionizing photon.

B. Analysis of intensities in the rotational spectra of HCl: Determination of the parameter *b*

Room-temperature rotationally resolved spectra obtained for mass 36 ($H^{35}Cl$) are shown in Figs. 1 and 2 for the $(E,0\text{-}X,0)$ and $(V,12\text{-}X,0)$ transitions, respectively. For both spectra the P and the R lines are absent, as expected for the two-photon $\Sigma \rightarrow \Sigma$ transition, while the O and S branches are significantly weaker than the Q branch. The ratios of the intensities I_O, I_Q, and I_S of the O, Q, and S rotational branches starting from the same ground rotational state J_i were used for determination of the $|b|^2$ value according to Eqs. (17) and (18).

The line intensities were obtained by integration of Gaussian functions which were used for fitting of the isolated rotational lines. For both transitions the $|b|^2$ values were
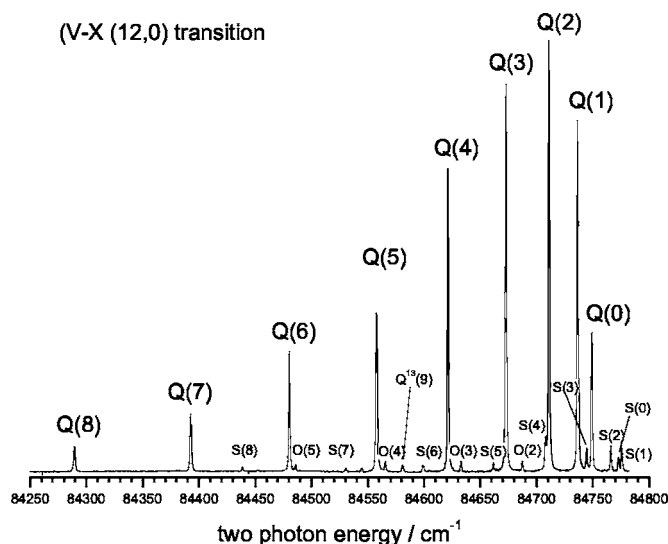

FIG. 1. REMPI detection of Cl^+: rotationally resolved and isotopically pure spectra at $T=300$ K of the transition $X(^1\Sigma^+, v_i=0) \rightarrow V(^1\Sigma^+, v_f=12)$.

found to be independent of the respective J_i values; therefore the mean value of $|b|^2$ was obtained by averaging over all observed transitions within a vibrational band. The values of $|b|^2$ for the V and E bands were found to be

$$|b_V|^2 = 2.01 \pm 0.15 \quad \text{and} \quad |b_E|^2 = 1.06 \pm 0.22, \qquad (40)$$

respectively. Error ranges were obtained from averaging over nine lines $[O(2)\cdots O(5)$ and $S(0)\cdots S(3), S(5)]$ for the $(V\text{-}X)$ transition and eight lines $[O(2)\cdots O(4)$ and $S(0)\cdots S(4)]$ for the $(E\text{-}X)$ transition.

In general, the parameter b in Eq. (19) is a complex number and describes not only the relative contributions from parallel and perpendicular pathways to the two-photon absorption, but also possible phase shifts. However, for the $B(V,E) \leftarrow X$ transitions in HCl, the parameter can be assumed as real because the photon frequency ω in the denominator in Eqs. (20) and (21) is out of resonance with the nearest intermediate molecular state $A\,^1\Pi$ (see potential en-
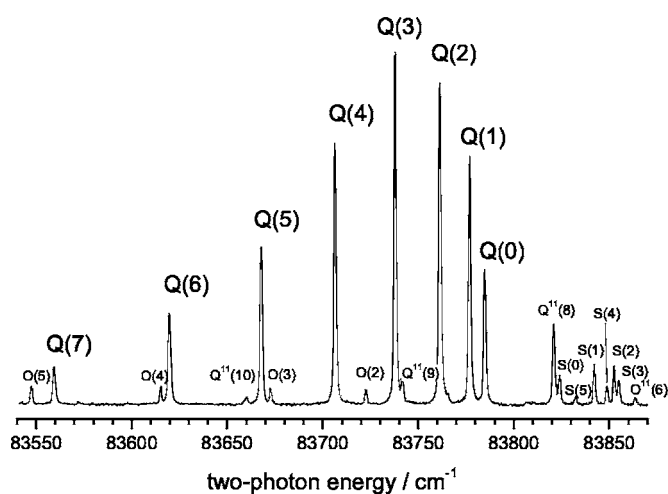

FIG. 2. REMPI detection of Cl^+: rotationally resolved and isotopically pure spectra at $T=300$ K of the transition $X(^1\Sigma^+, v_i=0) \rightarrow E(^1\Sigma^+, v_f=0)$.
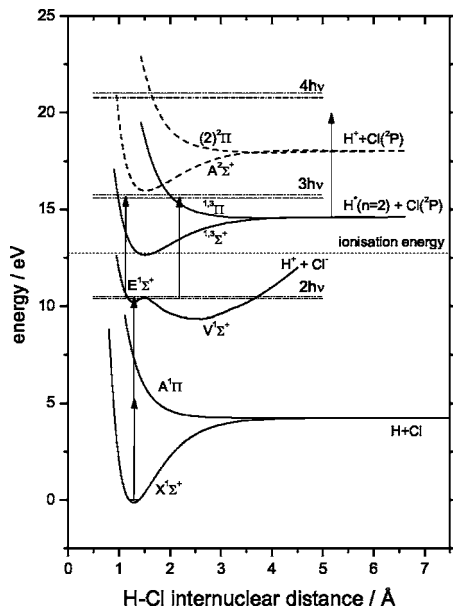
FIG. 3. Selected potential energy curves for HCl and HCl⁺. The ionic state $X\,^2\Pi$ is shown by the dashed curve. According to Ref. 19, the production of Cl+H* and H+Cl* products is mainly due to excitation of repulsive states of HCl** which are shown in this figure. Horizontal lines show the ionization energy (dotted line) and the photon energies, dashed and dash-dotted for $(V, 12\text{-}X, 0)$ and $(E, 0\text{-}X, 0)$ transitions, respectively. The first two-photon step is shown by the vertical arrow. The curves for $X\,^1\Sigma^+$, $a\,^3\Pi$, $A\,^1\Pi$, $C\,^1\Pi$, and $t\,^3\Sigma^+$ are taken from the paper of Alexander *et al.* (Ref. 48).

ergy curve diagram in Fig. 3). This conclusion is also in agreement with our experiment, which showed no photofragments produced in direct photodissociation via the $A\,^1\Pi$ state by 236 nm radiation. Therefore, in the conditions of our experiment the real part of b was larger than the imaginary part and likely dominated in the two-photon absorption.

The coefficient squares in Eq. (40) do not give any information about the *sign* of the parameter b, which determines the excited state alignment, as shown in Eq. (25). As shown below, the parameter b is most likely positive for both $V \leftarrow X$ and $E \leftarrow X$ transitions because only the positive sign fits with our experimental photofragment angular distribution. Assuming that b is positive, we get the following relationship for the intensities of the parallel and perpendicular pathways in two-photon transitions [(20) and (21)]

$$\frac{|D_\perp|^2}{|D_\parallel|^2} = 85 \pm 17 \tag{41}$$

for the V band and

$$\frac{|D_\perp|^2}{|D_\parallel|^2} \simeq 10^4 \tag{42}$$

for the E band.

These results show that for both V and E bands the two-photon excitation proceeds mainly through the perpendicular channel which is also in agreement with the potential curve diagram in Fig. 3, where the $A\,^1\Pi$ state is the nearest one to the single-photon energy.

A similar procedure was used for the determination of the branching ratio between the parallel and perpendicular pathways for the $X\,^1\Sigma \rightarrow B\,^1\Sigma$ transition in HCl by Kvaran *et*

al.[10] and for the $X\,^1\Sigma_g \rightarrow E, F\,^1\Sigma_g$ transitions in H₂ by Marinero *et al.*[26] Contrary to our result, Kvaran *et al.* reported a major contribution from the parallel-type transitions. We do not know the reason for this disagreement and can only assume that experimental conditions in the work of Kvaran *et al.* were different from ours, particularly maybe due to saturation of the absorption transitions.

C. Determination of the intermediate state alignment

Two nonzero components of the $^1\Sigma$, $J_f = 1$ excited state multipole ρ_{KQ} are given in Eqs. (24) and (25). It is shown that the "population" state multipole ρ_{00} depends on the square of the parameter b, while the "alignment" state multipole ρ_{20} depends on the real part of this parameter. The alignment parameter A_{20} of the angular momentum J_f can be calculated in terms of the parameter b as

$$A_{20} = \left[\frac{(2J_f + 3)(2J_f - 1)}{5J_f(J_f + 1)}\right]^{1/2} \frac{\text{Re}[\rho_{20}]}{\rho_{00}} = \frac{10\,\text{Re}[b] - 1}{25|b|^2 + 2}. \tag{43}$$

In case the perpendicular channel dominates ($b \simeq 1$), the alignment parameter in Eq. (43) is equal to $A_{20} \simeq 1/3$. In case the parallel channel dominates ($b \simeq -1/2$), it is equal to $A_{20} \simeq -8/11$. These values can be compared with the extremal values of the alignment parameter A_{20}: $A_{20}^{\max} = 1/2$, $A_{20}^{\min} = -1$.[28] In the former case the molecular axes are mostly perpendicular to the light polarization, while in the latter case they are mostly parallel to the light polarization, showing the same behavior as for a one-photon transition. However, contrary to the case of a one-photon transition, pure perpendicular and pure parallel channels do not lead to the extremal possible values of the alignment parameter. According to Eq. (43), the maximum and minimum possible values of A_{20} can be achieved with a certain mixture of the parallel and perpendicular pathways, when $b = 2/5$ and $b = -1/5$, respectively.

Using the values of $|b_V|^2$ and $|b_E|^2$ given above and choosing a positive sign of b, we obtained $A_{20}(V) = 0.252 \pm 0.008$ and $A_{20}(E) = 0.326 \pm 0.025$ which means that the population of the $M_f = \pm 1$ magnetic substrates is larger than the population of the $M_f = 0$ substrate.

The corresponding axis angular distribution is given in Eqs. (29) and (30) where the effective β^f parameters can be obtained from $\beta_V^f = -0.504 \pm 0.016$ and $\beta_E^f = -0.65 \pm 0.05$. These values indicate that for both channels the molecular axes are aligned predominantly perpendicular to the direction of light polarization which is also in agreement with the potential curve diagram in Fig. 3, where the $A\,^1\Pi$ state is the nearest one to the single-photon energy.

D. 3D imaging results: Photofragment angular distributions

Three-dimensional distributions of H⁺ ions generated in the photodissociation of jet-cooled HCl were obtained at four wavelengths corresponding to $Q(0)$ and $Q(1)$ rotational transitions for each of $(E, 0\text{-}X, 0)$ and $(V, 12\text{-}X, 0)$ vibrational transitions. Examples of such speed distributions observed
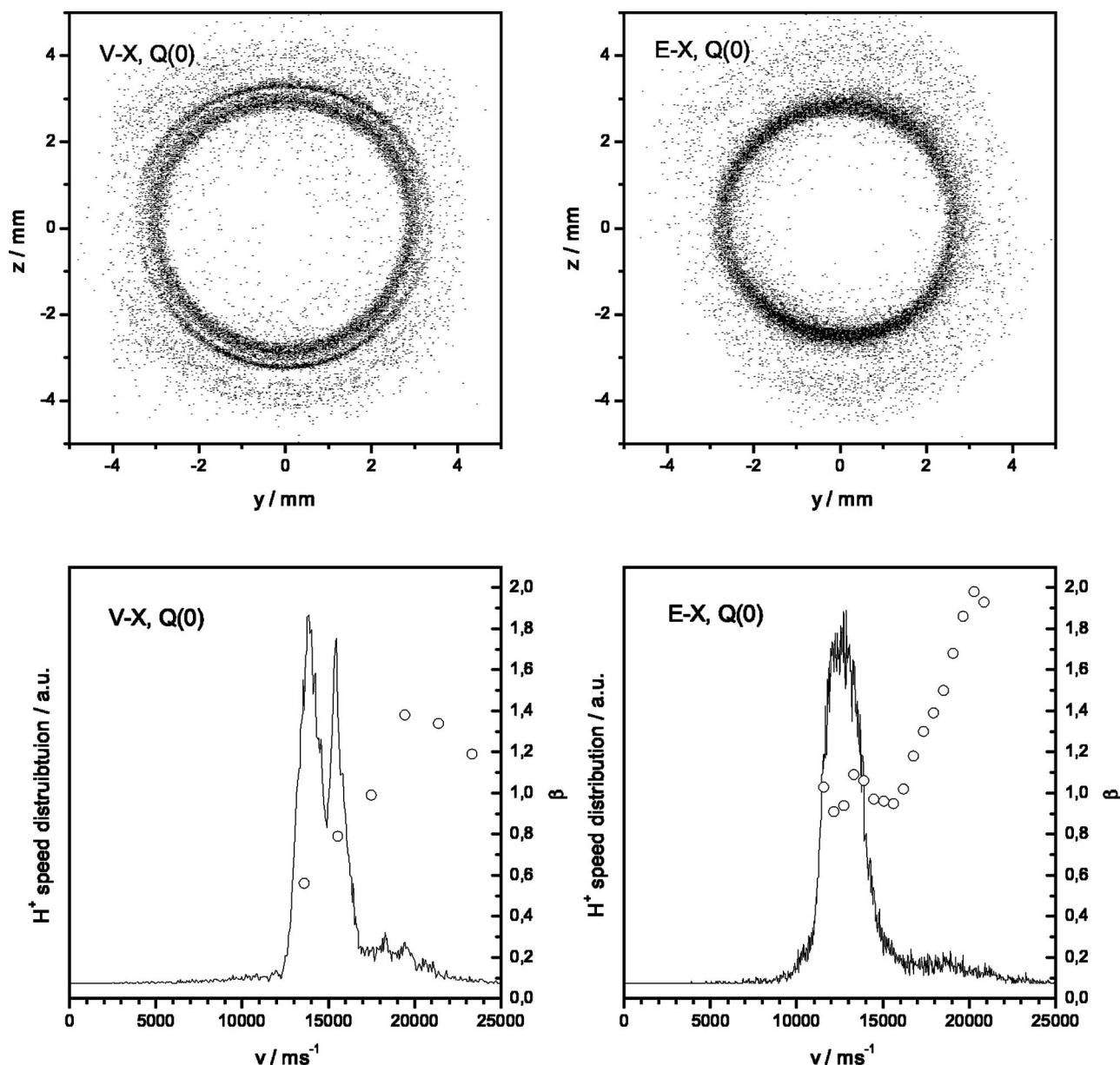
FIG. 4. Top: Examples of two-dimensional projections of 3D images obtained for $Q(0)$ transitions for *V-X* (left) and *E-X* (right) excitations. Bottom: The corresponding speed and spatial distributions obtained from 3D images by the procedure outlined in Ref. 19. Compared to the data shown in Ref. 19, the resolution displayed here has significantly been improved by the use of a slit limiting the lateral dimension of the molecular beam, thus reducing the size of the interaction volume of the laser and the molecular beams.

for both vibrational transitions are shown in Fig. 4 together with corresponding two-dimensional projections of the raw three-dimensional images. A detailed discussion of projection procedures and data analysis can be found in our recent paper.[19] We would like to point out, however, that reconstruction methods have not been applied, neither to the presentation in Fig. 4, nor in the data analysis. The only data treatment performed in Fig. 4 is an inevitable projection of the experimentally obtained three-dimensional images to the two-dimensional world of a paper journal.

In both cases we observed "fast" and "slow" groups of ions, from REMPI $(2+1_i+1)$ and $(2+1+1_i)$, respectively, as explained above. The resulting three-dimensional images integrated over the polar angle ϕ were fitted with the function[16]

$$F(\theta) = A \sin\theta[1 + \beta_2 P_2(\cos\theta) + \beta_4 P_4(\cos\theta)], \qquad (44)$$

where A, β_2, and β_4 are fitting parameters. Please note that this fitting procedure is directly applied to the observed three-dimensional image and does not rely on any reconstruction methods. Physically, the Legendre polynomials up to rank $K=6$ and even more may be needed to describe the angular distribution, having in mind possible contribution from initial anisotropy in the molecular beam, alignment of the molecular excited states, and the following multiphoton fragmentation. However, we found that the contribution from the additional $\beta_6 P_6(\cos\theta)$ term in Eq. (44) could not be accurately extracted from the experimental data.

The fitting parameters β_2 and β_4 which were determined from the experimental images with Eq. (44) are presented in

TABLE I. Summary of experimental and calculated values of the β_2 and β_4 fitting parameters obtained from fitting of angular distributions of H$^+$ ions with Eq. (44).

Transition	$V\,^1\Sigma^+ \leftarrow X\,^1\Sigma^+$ averaged values		$E\,^1\Sigma^+ \leftarrow X\,^1\Sigma^+$ slow ions		$E\,^1\Sigma^+ \leftarrow X\,^1\Sigma^+$ fast ions	
Rotational line	$Q(0)$	$Q(1)$	$Q(0)$	$Q(1)$	$Q(0)$	$Q(1)$
β_2	1.00 ± 0.16	0.28 ± 0.08	1.14 ± 0.04	0.42 ± 0.12	1.56 ± 0.43	1.26 ± 0.22
β_4	-0.19 ± 0.10	-0.57 ± 0.25	-0.29 ± 0.13	-0.76 ± 0.17	0.06 ± 0.10	-0.22 ± 0.17
β_2^{cal}		0.42 ± 0.16		0.387 ± 0.085		0.76 ± 0.50
β_4^{cal}		-0.47 ± 0.11		-0.73 ± 0.13		-0.59 ± 0.25

Table I. It is clear from Table I that in experiment the parameters β_2 and β_4 are significantly reduced for the $Q(1)$ transitions in comparison to their values for the $Q(0)$ transitions. This reduction is due to the excited state alignment of the angular momentum $J_f=1$. Using Eq. (29)–(31) and Eq. (44) we conclude that only the positive value of the parameter b is in agreement with the obtained result. Note that a positive value of b corresponds to the *negative* value of β in Eq. (29).

Equation (28) clarifies the role of the excited state alignment on the fragment angular distribution. It shows that the angular distribution of the photofragments produced via the transition $|f\rangle \rightarrow |c\rangle$ can be presented as a product of the angular distribution of the molecular axes $\omega_f(\mathbf{n})$ in the $|f\rangle$ state and the photofragment angular distribution $\omega_{\mathrm{ph}}^{(k)}(\mathbf{n},\mathbf{n}_{\mathrm{ph}})$ resulting from photodissociation of the *unpolarized* $|f\rangle$ state, which depends on the transition moments and on the light polarization, but not on the J_f value.

Therefore, the angular distribution $\omega_{\mathrm{ph}}^{(1)}(\mathbf{n},\mathbf{n}_{\mathrm{ph}})$ is the same for the $Q(0)$ and $Q(1)$ transitions and is given by the experimental data for the $Q(0)$ transitions in Table I. We calculated the molecular axis angular distribution $\omega_f(\mathbf{n})$ for the $Q(1)$ transitions from Eqs. (29) and (30) using the values of the b parameters and then determined the angular distributions for the $Q(1)$ transition with respect to Eq. (28). The obtained angular distributions were presented in the form (44), where the two last items are proportional to the parameters β_2^{cal} and β_4^{cal}, the values of which are given in Table I. As can be seen from Table I, the calculated values of the β_2 and β_4 parameters are in excellent agreement with the experimental values.

Romanescu et al.[17] have determined the β_2 parameters by REMPI for slow H$^+$ ions for $(E,0\text{-}X,0)$; $Q(1)$ transitions are 0.9 and -0.2 for channels producing Cl($^2P_{1/2}$)+H* and Cl($^2P_{3/2}$)+H*, respectively. From Fig. 5(a) of Romanescu et al. it is clear that the second channel has a very small probability in comparison with the probability of the first channel. Hence Romanescu et al.[17,18] obtained $\beta_2 \approx 0.9$. We fitted our experimental data in the same way as Romanescu et al., neglecting the item with β_4, and obtained the value of $\beta_2 = 0.8\pm0.1$, in good agreement with Romanescu et al.

For the same transition Manzhos et al.[18] report $\beta_2 = 1.04$ and $\beta_4 = -0.67$.

E. Higher order effects

Note that the experimental β_4 parameters are not equal to zero for $Q(0)$ transitions, in contradiction to the fact that the alignment of HCl* is obviously zero for the $Q(0)$ transition and one-photon dissociation steps [(35) and (39)] cannot produce angular distribution with Legendre polynomials with rank $K>2$. We resolve this contradiction as follows. The duration of the laser pulse is rather large (3–5 ns), and the speed of the excited H*($n=2$) atoms is also large (~20 km/s). Hence, the atoms can fly outside of the laser spot (diameter ~10 μm) during the laser pulse, and the REMPI detection may have a preference to H* atoms flying along the laser beam, in comparison with atoms flying perpendicular to the laser beam. This will result in the observation of a distorted angular distribution of the ions, with a lack of ions in the directions of the electric vector of the laser radiation, at $\theta\sim0$ and $\theta\sim\pi$. This lack leads to nonzero β_4 parameters in Eq. (44). This explanation is appropriate only for slow H$^+$ ions, but it does not work for fast ions, which are produced by photodissociation of very slow HCl$^+$ ions. From the Table I it can be seen that for the $Q(0)$ transitions the β_4 parameters are relatively large for slow ions and close to zero for fast ions, in agreement with the explanation.

F. Anisotropy in the molecular beam

In principle, the 3D imaging technique allows us also to study the alignment of HCl in the molecular beam prior to photon absorption. Such alignment has been observed for a variety of molecules, and such alignment cannot *a priori* be considered to be absent. While the general theory outlined in the previous sections is applicable to aligned and nonaligned species likewise, the values for the experimentally observed β parameters must be different for different polarization directions of the excitation laser. Note that the presence of such alignment is a serious problem for imaging methods relying on reconstruction methods, while the 3D imaging technique is ideally suited for its study.

However, from the comparison of the angular distributions of H$^+$ ions obtained for $Q(1)$ transitions for both laser polarizations, we conclude that under our experimental conditions the alignment of HCl in the molecular beam is small, and an upper limit may be established as $|A_{20}|<0.1$.

V. SUMMARY

The results can be summarized as follows.

- 3D velocity (speed and angle) distributions of H$^+$ ions have been compared for the $Q(0)$ and $Q(1)$ rotational transitions of the $(E,0\text{-}X,0)$ and $(V,12\text{-}X,0)$ vibrational

transitions. From the analysis of these distributions we have obtained β_2 parameters, which are large and positive. We have observed a decrease of β_2 parameters in the $Q(1)$ transition in comparison to the $Q(0)$ transition, $\beta_2(Q(1)) \lesssim \beta_2(Q(0))$, for both vibrational transitions. We expect that this decrease is due to the alignment of the excited $HCl^*(J_f=1)$ molecule, which is produced via the $Q(1)$ transition in the two-photon step (34). This alignment is absent for the $Q(0)$ transition, since the $J_f=0$ rotational state is isotropic. The alignment is due to the perpendicular nature of the two-photon step (34) which occurs via the $^1\Sigma \rightarrow {}^1\Pi \rightarrow {}^1\Sigma$ pathway, where the virtual intermediate state is the $A\ ^1\Pi$ state.

- A detailed theory of the alignment in the two-photon transition process is presented.

- REMPI $(2+1_i)$ rotational spectra of HCl^+ were recorded by a one-dimensional TOF mass spectrometry. Ratios of intensities of rotational lines of O, Q, and S branches originating from the same ground state level J_i were used to determine the values $|b_V|^2 = 2.01 \pm 0.15$ and $|b_E|^2 = 1.06 \pm 0.22$ for $(E,0-X,0)$ and $(V,12-X,0)$ transitions, respectively. Using these values of $|b_V|^2$ and $|b_E|^2$, we obtained alignment parameters $A_{20}(V) = 0.252 \pm 0.008$ and $A_{20}(E) = 0.326 \pm 0.025$.

- Our 3D imaging techniques is very suitable for study of alignment in the molecular beam. However, no such alignment was found under our experimental conditions in the HCl/He molecular beam.

ACKNOWLEDGMENTS

APPENDIX A: TRANSFORMATION OF THE LIGHT POLARIZATION MATRIX E_{KQ}

The light polarization matrix E_{KQ} is defined by[28]

$$E_{KQ} = [\mathbf{e} \otimes \mathbf{e}^*]_{KQ}$$
$$= \sum_{\mu\mu'} C^{KQ}_{1\mu1\mu'} e_\mu (\mathbf{e}^*)_{\mu'}$$
$$= \sum_{\mu\mu'} (-1)^{\mu'} C^{KQ}_{1\mu1-\mu'} e_\mu e^*_{\mu'}, \qquad (A1)$$

where $\mathbf{e}$ is the light polarization vector which is in general complex.

The polarization index $\mu = 0, \pm1$ in Eq. (A1) specifies

cyclic coordinates of the vector $\mathbf{e}$. If the Z axis is parallel to the $\mathbf{e}$ vector of the linearly polarized light, the only nonzero projection is $e_0 = 1$, while the projections $e_{\pm1}$ are both equal to zero. If the Z axis is parallel to the direction of propagation of the circularly polarized light, the only nonzero projections are $e_{-1} = 1$ and $e_1 = 1$ for right- and left-hand polarization, respectively. We will call the above choice as photon frame. Expanding the components e_μ for linearly or circularly polarized light defined in an arbitrary coordinate frame over the photon frame components e_s, we get

$$e_\mu = D^{1\,*}_{\mu s}(\varphi, \vartheta, 0), \qquad (A2)$$

where the angles φ and ϑ specify the vector $\mathbf{n}_{ph}$ which is parallel to the light polarization vector in the case of linearly polarized light and to the direction of light propagation in the case of circularly polarized light. $D^1_{\mu s}(\varphi, \vartheta, 0)$ in Eq. (A2) is a Wigner rotation function[32] where the index s is equal to $s = 0$ for linearly polarized light and to $s = -1$ and $s = 1$ for right- and left-hand circularly polarized light, respectively.

Substituting (A2) into (A1), using the Clebsch-Gordan series,[28] and proceeding with the summation over the indices μ, μ', we get

$$E_{KQ} = \sum_{\mu\mu'} (-1)^{\mu'} C^{KQ}_{1\mu1-\mu'} D^{1\,*}_{\mu s}(\mathbf{n}_{ph}, 0) D^1_{\mu's}(\mathbf{n}_{ph}, 0)$$
$$= (-1)^s C^{K0}_{1s1-s} D^{K\,*}_{Q0}(\mathbf{n}_{ph}, 0)$$
$$= (-1)^s C^{K0}_{1s1-s} C_{KQ}(\mathbf{n}_{ph}). \qquad (A3)$$

APPENDIX B: CALCULATION OF THE TWO-PHOTON EXCITATION MATRIX $F_{K_fQ_f}(J_fJ'_f)$

In the Born-Oppenheimer approximation each of the matrix element of the electromagnetic interaction operator $\hat{V} = \mathbf{d} \cdot \mathbf{e}$ in Eq. (2) can be written as

$$\hat{V}_{ji} = \sum_{p,q} (-1)^p e_p \langle J_j M_j \Omega_j | D^{1\,*}_{-pq}(\mathbf{n}, 0) | J_i M_i \Omega_i \rangle$$
$$\times \langle n_j v_j \Omega_j | \hat{d}_q | n_i v_i \Omega_i \rangle, \qquad (B1)$$

where vector $\mathbf{n} \equiv \mathbf{n}(\phi, \theta)$ describes the direction of the molecular axis. Indices $p = 0, \pm1$ specify cyclic projection of vector $\mathbf{e}$ onto the *laboratory frame*, while the indices $q = 0, \pm1$ specify the projection of vector $\mathbf{d}$ onto the *molecular frame*.

Two terms in the square brackets in Eq. (B1) represent rotational and electronic/vibrational matrix elements. Substituting Eq. (B1) into Eq. (2), evaluating integrals over the angles ϕ and θ in the rotational matrix elements, making transformation to the irreducible representation of the density matrix through Eqs. (3) and (4), and proceeding with the summation over the indices M_i, M'_i, M_e, M'_e, M_f, M'_f, J_e, and J'_e using the summation rules of quantum angular momentum theory,[32] the expression for the two-photon excitation matrix

$F_{K_f Q_f}(J_f J_f')$ can be presented in the following form:

$$F_{K_f Q_f}(J_f J_f') = F_0 \sum_{K K_1 K_2 K_i} ((E_{K_1} \otimes E_{K_2})_K \otimes \rho_{K_i}(J_i J_i'))_{K_f Q_f} S_{K_i K_1 K_2}^{K K_f},$$

$$(B2)$$

where $E_{K_1 Q_1}$ and $E_{K_2 Q_2}$ are polarization matrices[28] of the first and the second photons with their ranks K_1 and K_2 and projections Q_1 and Q_2, respectively, $\rho_{K_i Q_i}(J_i J_i')$ is a state multipole of the initial state, and the term in parentheses is the double vector product.[32] The scalar factor $S_{K_i K_1 K_2}^{K K_f}$ is

$$S_{K_i K_1 K_2}^{K K_f} = (-1)^{K_1 + K_2 + J_f' - J} [(2K_1 + 1)(2K_2 + 1)(2K + 1)(2K_i + 1)(2J_f' + 1)(2J_f + 1)]^{1/2} \sum_{R R', J_i J_i'} [(2J_i' + 1)(2J_i + 1)$$

$$\times (2R' + 1)(2R + 1)]^{1/2} \begin{Bmatrix} J_i & J_f & R \\ J_i' & J_f' & R' \\ K_i & K_f & K \end{Bmatrix} \begin{Bmatrix} 1 & 1 & R \\ 1 & 1 & R' \\ K_1 & K_2 & K \end{Bmatrix} \sum_\gamma (-1)^{R'+R} \begin{pmatrix} J_i' & R' & J_f' \\ \Omega_i & \gamma & -\Omega_f \end{pmatrix} \begin{pmatrix} J_i & R & J_f \\ \Omega_i & \gamma & -\Omega_f \end{pmatrix} S_{R'\gamma} S_{R\gamma}^*, \quad (B3)$$

where the terms in the curly braces are $9-j$ symbols.[32]

Equation (B2) generalizes Eq. (3) given by Manzhos *et al.* in Ref. 18 to the case of a polarized molecular ground state, and it is also written for the case when two photons are not necessary the same. In the case of the unpolarized ground state and the same photons Eqs. (B2) and (B3) are in principle equivalent to the corresponding expressions of Manzhos and *et al.*;[18] however, they are presented in our paper in a different form. The reason is that the standard definition of the light polarization matrix we use in Eq. (A1) differs from the definition used by Manzhos *et al.*

If the light is linearly or circularly polarized, the matrices $E_{K_1 Q_1}$ and $E_{K_2 Q_2}$ in Eq. (B2) can be presented in the form (A3). Assuming that both photons are the same, after substitution of these expressions into Eq. (B2), applying the Clebsch-Gordan series, and proceeding with the summation over the indices Q_1, Q_2, K_1, and K_2, the two-photon excitation matrix can be presented as in Eq. (6).

APPENDIX C: ANGULAR DISTRIBUTION OF THE MOLECULAR AXIS AFTER EXCITATION TO THE CONTINUUM ENERGY STATES

1. One-photon excitation

The state multipole describing a dissociative molecular state $|c\rangle$ after one-photon excitation from a discrete energy state $|f\rangle$ can be written as

$$\rho_{K_c Q_c}(J_c J_c')$$

$$\sim F_{K_c Q_c}(J_c J_c')$$

$$= F_0 \sum_{K_f K_1} (-1)^{K_1 + J_c - J_c' + 1} [E_{K_1} \otimes \rho_{K_f}]_{K_c Q_c}(2J_f + 1)$$

$$\times [(2K_f + 1)(2K_1 + 1)]^{1/2} \begin{Bmatrix} K_c & K_1 & K_f \\ J_c & 1 & J_f \\ J_c' & 1 & J_f \end{Bmatrix}$$

$$\times C_{J_f \Omega_f 1 q'}^{J_c' \Omega_c'} C_{J_f \Omega_f 1 q}^{J_c \Omega_c} \langle n_c v_c \Omega_c | d_q | n_f v_f \Omega_f \rangle^*$$

$$\times \langle n_c' v_c' \Omega_c' | d_{q'} | n_f v_f \Omega_f \rangle, \quad (C1)$$

where $\rho_{K_f Q_f}$ is the state multipole of the discrete energy state ($B\ ^1\Sigma$) with total angular momentum J_f and $E_{K_1 Q_1}$ is the photon polarization matrix.

Substituting Eq. (C1) into Eq. (27) where the quantum numbers K, J, and Ω are replaced by K_c, J_c, and Ω_c and proceeding with the summation over the indices J_c and J_c', the expression for the fragment angular distribution can be written as

$$\omega(\mathbf{n}) = (-1)^{K_1 - q + J_f - \Omega_f} \frac{(2J_f + 1)}{4\pi}$$

$$\times \sum_{K_c, K_1, K_f} ([E_{K_1} \otimes \rho_{K_f}]_{K_c} \cdot C_{K_c}(\mathbf{n}))$$

$$\times C_{K_1 0 K_f 0}^{K_c 0} C_{J_f \Omega_f J_f - \Omega_f}^{K_f 0} C_{1 q 1 - q}^{K_1 0} |\langle n_c \Omega_c | d_q | n_f \Omega_f \rangle|^2,$$

$$(C2)$$

where the term in the parentheses is a vector-scalar product:

$$([E_{K_1} \otimes \rho_{K_f}]_{K_c} \cdot C_{K_c}(\mathbf{n}))$$

$$= \sum_{Q_f, Q_1, Q_c} C_{K_1 Q_1 K_f Q_f}^{K_c Q_c} E_{K_1 Q_1} \rho_{K_f Q_f} C_{K_c Q_c}^*(\mathbf{n}). \quad (C3)$$

Using in Eq. (C2) the Clebsch-Gordan series for spherical harmonics, summation over the indices K_c and Q_c can proceed, which finally gives Eq. (28) where the term $\omega_c(\mathbf{n})$ is given in Eq. (31).

2. Two-photon excitation

A similar procedure as before can be used in the case of two-photon dissociation from a discrete energy state. The excitation matrix for two-photon excitation from state $|f\rangle$ to state $|c\rangle$ can be obtained from Eq. (6) by the exchange of the subscript indices $i \rightarrow f$ and $f \rightarrow c$. It can be substituted into the expression for axis distribution in Eq. (27) specified for the $|c\rangle$ state, and the result of the following summations can be written as

$$\omega(\mathbf{n}) = \frac{1}{4\pi} \sum (-1)^{R-\gamma+J_f-\Omega_f}(2J_f+1)$$

$$\times([C_K(\mathbf{n}_{ph}) \otimes \rho_{K_f}]_{K_c} \cdot C_{K_c}(\mathbf{n}))$$

$$\times C_{R2pR'-2p}^{K0}C_{1p1p}^{R2p}C_{1-p1-p}^{R'-2p}$$

$$\times C_{K0K_f0}^{K_c0}C_{R\gamma R'-\gamma}^{K0}C_{J_f\Omega_f J_f-\Omega_f}^{K_f0}S_{R'\gamma}S_{R\gamma}^*, \tag{C4}$$

where summation proceeds-over all repeated indices.

Using the explicit form of the vector-scalar product in Eq. (C4) and applying the Clebsch-Gordan series for spherical harmonics after some transformations the photofragment angular distribution can be presented in the form (28) where the term $\omega_c(\mathbf{n})$ is given in Eq. (32).

[1] S. Arepalli, N. Presser, D. Robie, and R. J. Gordon, Chem. Phys. Lett. **118**, 88 (1985).

[2] R. Callaghan, S. Arepalli, and R. J. Gordon, J. Chem. Phys. **86**, 5273 (1987).

[3] T. A. Spiglanin, D. W. Chandler, and D. H. Parker, Chem. Phys. Lett. **137**, 414 (1987).

[4] E. de Beer, B. G. Koenders, M. P. Koopmans, and C. Lange, J. Chem. Soc., Faraday Trans. **86**, 2035 (1990).

[5] D. S. Green, G. A. Bickel, and S. C. Wallace, J. Mol. Spectrosc. **150**, 303 (1991).

[6] D. S. Green, G. A. Bickel, and S. C. Wallace, J. Mol. Spectrosc. **150**, 354 (1991).

[7] D. S. Green, G. A. Bickel, and S. C. Wallace, J. Mol. Spectrosc. **150**, 388 (1991).

[8] Y. Xie, P. T. A. Reilly, S. Chilukuri, and R. J. Gordon, J. Chem. Phys. **95**, 854 (1991).

[9] D. S. Green and S. C. Wallace, J. Chem. Phys. **96**, 5857 (1992).

[10] A. Kvaran, A. Logadottir, and H. Wang, J. Chem. Phys. **109**, 5856 (1998).

[11] K. Wang and V. McKoy, J. Chem. Phys. **95**, 8718 (1991).

[12] E. Beer, W. J. Buma, and C. Lange, J. Chem. Phys. **99**, 3252 (1993).

[13] M. Penno, A. Holzwarth, and K.-M. Weitzel, Mol. Phys. **97**, 43 (1999).

[14] M. Michel, M. V. Korolkov, M. Malow, K. Brembs, and K.-M. Weitzel, Phys. Chem. Chem. Phys. **3**, 2253 (2001).

[15] A. Kvaran and H. Wang, Mol. Phys. **100**, 3513 (2002).

[16] A. Chichinin, K.-H. Gericke, T. S. Einfeld, and C. Maul, *Imaging in Molecular Dynamics: Technology and Applications* (Cambridge University Press, Cambridge, 2003), p. 138.

[17] C. Romanescu, S. Manzhos, D. Boldovsky, J. Clarke, and H.-P. Loock, J. Chem. Phys. **120**, 767 (2004).

[18] S. Manzhos, C. Romanescu, H.-P. Loock, and J. G. Underwood, J. Chem. Phys. **121**, 11802 (2004).

[19] A. Chichinin, C. Maul, and K.-H. Gericke, J. Chem. Phys. **124**, 224324 (2006).

[20] R. Bray and R. Hochstrasser, Mol. Phys. **31**, 1199 (1976).

[21] A. Bain and A. McCaffery, J. Chem. Phys. **83**, 2641 (1985).

[22] A. Kummel, G. Sitz, and R. Zare, J. Chem. Phys. **85**, 6874 (1986).

[23] A. Kummel, G. Sitz, and R. Zare, J. Chem. Phys. **88**, 6707 (1987).

[24] A. Bracker, E. Wouters, A. Suits, and O. Vasyutinskii, J. Chem. Phys. **110**, 6749 (1999).

[25] A. G. Smolin, O. S. Vasyutinskii, E. R. Wouters, and A. G. Suits, J. Chem. Phys. **121**, 1 (2004).

[26] E. Marinero, R. Vasudev, and R. Zare, J. Chem. Phys. **78**, 692 (1983).

[27] E. R. Wouters, M. Ahmed, D. S. Peterka, A. S. Bracker, A. G. Suits, and O. S. Vasyutinskii, in *Imaging in Chemical Dynamics*, edited by R. E. Continetti and A. G. Suits (American Chemical Society, Washington, 2000), p. 238.

[28] R. N. Zare, *Angular Momentum* (Wiley, New York, 1988).

[29] R. N. Dixon, J. Chem. Phys. **122**, 194302 (2005).

[30] W. Happer, Rev. Mod. Phys. **44**, 169 (1972).

[31] K. Blum, *Density Matrix Theory and Applications*, 2nd ed. (Plenum, New York, 1996).

[32] D. Varshalovich, A. Moskalev, and V. Khersonskii, *Quantum Theory of Angular Momentum* (World Scientific, Singapore, 1988).

[33] Y. Mo and T. Suzuki, J. Chem. Phys. **109**, 4691 (1998).

[34] M. Docker, Chem. Phys. **125**, 185 (1988).

[35] J. Underwood and I. Powis, J. Chem. Phys. **113**, 7119 (2000).

[36] E. B. Alexandrov, M. P. Chaika, and G. I. Khvostenko, *Interference of Atomic States* (Springer, Berlin, 1993).

[37] L. D. A. Siebbeles, M. Glass-Maujean, O. Vasyutinskii, J. Beswick, and O. Roncero, J. Chem. Phys. **100**, 3610 (1994).

[38] A. Chichinin, T. Einfeld, C. Maul, and K.-H. Gericke, Rev. Sci. Instrum. **73**, 1856 (2002).

[39] P. Natalis, P. Pennetreau, L. Longton, and J. E. Collin, Chem. Phys. **73**, 191 (1982).

[40] T. A. Carlson, M. O. Krause, A. Fahlman, P. R. Keller, J. W. Taylor, T. Whitley, and F. A. Grimm, J. Chem. Phys. **79**, 2157 (1983).

[41] S. Svensson, L. Karlsson, P. Baltzer, B. Wannberg, U. Gelius, and M. Y. Adam, J. Chem. Phys. **89**, 7193 (1988).

[42] H. Frohlich, P. M. Guyon, and M. Glass-Maujean, J. Chem. Phys. **94**, 1102 (1991).

[43] K. S. Haber, Y. Jiang, G. Bryant, and E. R. Grant, Phys. Rev. A **44**, R5331 (1991).

[44] R. G. Tonkyn, R. T. Wiedemann, and M. G. White, J. Chem. Phys. **96**, 3696 (1992).

[45] A. J. Yencha, A. J. Cormack, R. J. Donovan, A. Hopkirk, and G. C. King, Chem. Phys. **238**, 109 (1998).

[46] A. Yencha, G. King, M. Lopes, J. Bozek, and N. Berrah, Chem. Phys. Lett. **315**, 37 (1999).

[47] H.-P. Loock (private communication).

[48] M. Alexander, X. Li, R. Liyanage, and R. Gordon, Chem. Phys. Lett. **231**, 331 (1980).